Aalborg Universitet

Two-Order Deep Learning for Generalized Synthesis of Radiation Patterns for Antenna Arrays

Zhou, Zhao; Wei, Zhaohui; Ren, Jian; Yin, Yingzeng; Pedersen, Gert Frølund; Shen, Ming

Two-order Deep Learning for Generalized Synthesis of Radiation Patterns for Antenna Arrays

Zhao Zhou, Zhaohui Wei, Jian Ren, *Member, IEEE,* Yingzeng Yin, *Member, IEEE,* Gert Frølund Pedersen, *Senior Member, IEEE,* and Ming Shen, *Senior Member, IEEE*

Abstract—This letter tackles the generalized synthesis of antenna arrays using two-order deep learning. Existing deep learning-assisted antenna synthesis approaches mainly rely on model training using electromagnetic (EM) simulation data and hence feature limited generalization ability and the need for a huge amount of EM simulations. The proposed two-order deep learning method uses the first-order model to learn the generic features of radiation patterns from the data efficiently generated by applying conventional array factors. After that, the second-order model learns from EM simulations to capture the detailed pattern variations due to concrete coupling effects in the case of a specific array arrangement with different operating frequencies, radiation structures, and feeding schemes. Therefore the two-order DL model can predict the radiation patterns of a series of antenna arrays while reducing the needed amount of EM simulation data. Implementation was carried out on a series of patch antenna arrays to verify the feasibility and robustness of the proposed approach. The validation includes conditions for the array operating at arbitrary new frequencies, with modified radiation structures or new feeding schemes. The results show that the proposed two-order model provides a prediction accuracy of about 84% for a series of 1 by 4 antenna arrays, clearly outperforming the existing regular one-order DL model, which obtains around 65% with the same EM simulation data. The proposed method reveals a promising direction for applying deep learning to assist the design and analysis of antenna arrays.

Impact Statement—As the fifth/sixth (5G/6G) generation communication era approaches, radar and other wireless communication systems have been applied in many different scenarios. The antenna array is an essential component in these systems. The thorough analysis of the array under design calls for continuous monitoring of its radiation performance as a major feature. However, the conventional array factor-based calculation methods lack accuracy; the full-wave EM simulation is time-consuming; the existing deep learning-assisted approaches are single-array-oriented and have limited generalization ability. Therefore, an efficient generalized array radiation synthesis method is in great demand. We propose a wide-array-coverage-oriented deep learning solution for generalized radiation synthesis to achieve this. It is accomplished by a two-order deep neural network that combines the merits of array factor-based calculation and EM simulation. The two-order model reduces the need for simulation and improves the generalization ability. The well-trained model maintains compatibility and functionality for a series of antenna arrays with similar topology. This approach is
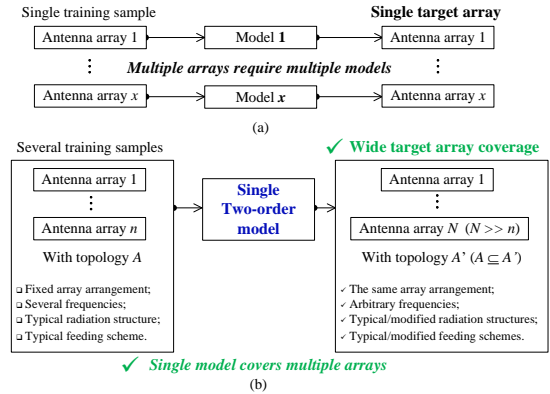
Fig. 1. Comparison of (a) published regular DL-based method and (b) the proposed DL-based two-order method for antenna array radiation synthesis.

a good complementary tool to analyze and conveniently examine the radiation performance of the antenna arrays.

Index Terms—antenna array, deep learning, deep neural network, generalized synthesis, two-order, radiation pattern.

I. INTRODUCTION

DEEP learning (DL) has shown the potential to solve complex, especially non-analytic problems, such as face or speech recognition and image classification. The DL-based beyond-5G/6G (beyond-fifth/sixth communication generation) solutions have significantly inspired both academia and industry, including smart wave management, imperfect channel estimation [1–10], direction-of-arrival estimation [11–13], inverse scattering [14–20], inverse design of microwave components [21–23], and array radiation synthesis [24–28].

Wireless communication systems have been widely applied in many scenarios, such as self-driving vehicles, remote surgery, home automation, indoor localization, etc. [29]. Wireless communication systems rely on a well-behaved antenna array. In the design and analysis of antenna arrays, the array radiation is a core indicator. To constantly monitor this indicator, the whole analysis process will witness repetitive procedures of array radiation synthesis. Thus, a convenient generalized array synthesis method is required. A traditional way is to calculate radiation with the element radiation pattern and excitation condition based on the array factor. It is convenient and computationally low cost, yet inaccurate to describe non-ideal array characteristics such as coupling effects, which can hardly be generalized with closed-loop expressions. Thus, the oriented array must be modeled and simulated via EM simulation software to synthesize its radiation pattern. EM simulation

provides high accuracy by paying a high computation cost. On the one hand, the computation complexity might be tolerable for small-scale antenna arrays but is sometimes tricky to handle with ordinary hardware when it comes to large-scale antenna arrays.

On the other hand, its computation is non-reusable because any tiny modification to the structure could void the existing results and require a new simulation. In general, it could take many changes to reach an optimal design, and thus often, many simulation iterations are needed. In this way, deep learning may help significantly accelerate the whole design process by re-using the former simulation results. After being trained with the former simulation results, deep neural networks can predict the future array's radiation patterns at a low computation cost.

Radial basis function neural networks were employed in [24] to estimate the directivity for linear dipole arrays. Similarly, the authors in [25] used a multibranch ANN to solve the inverse problem of the antenna array directivity. However, in most cases, we need more detailed information on the whole array radiation pattern to evaluate beamwidth, sidelobe suppression, etc.

The authors of [26–28] managed to apply deep learning for radiation synthesis, where [26] presented a neural network-based (NN) method capable of establishing a relation between input voltages for all elements and radiation patterns of the target array. The NN they used as a black box considered the interference between elements and possible obstacles positioning within the radiating area. The solution published in [27] focused on the mutual coupling between antenna elements. NN was proven able to exploit the hidden principle of radiation to predict the voltages needed to generate given radiation patterns. Instead of NN, [28] investigated the possibility of applying a deep neural network (DNN) for antenna array radiation synthesis. All the three methods from [26–28] can imitate the mapping between the excitation conditions and the antenna arrays' radiation patterns. However, as illustrated in Fig. 1(a), they are single-array-oriented methods; the well-trained models can only exclusively serve for one specific antenna array. That means every array calls for an exclusive model, and we need to perform the whole process of model generation for each array. For the sake of higher efficiency, generalized synthesis methods are in great demand, which is precisely the motivation for us to develop a wide-array-coverage-oriented generalized synthesis method.

This letter proposes a wide-array-coverage-oriented deep learning solution for the generalized antenna array radiation synthesis. We have two main contributions: 1) compared to the regular model only serving for one exclusive array, the proposed two-order model inspired by electromagnetic theory can offer generalized radiation synthesis for a series of antenna arrays once being trained with several array samples, as demonstrated in Fig. 1; 2) unlike most existing deep learning methods heavily relying on simulation, we significantly alleviate the burden on simulation by taking advantage of well-established array factors [30]. As the name suggests, the two-order model incorporates a two-order training process. In advance, we train a conventional fully-connected deep neural network to grab the generic radiation patterns of a group of target antenna arrays, with massive theoretical data handily collected via array factors. The model is then elevated into a two-order model and trained using EM simulation data to improve the accuracy for customized array designs. Thus, the first-order model can learn the basic features of radiation synthesis. The second-order model can then capture the detailed radiation variations due to concrete coupling effects in the customized arrays: specific array arrangements with different operating frequencies, radiation structures, and feeding schemes. We verified the proposed method's feasibility, performance, and robustness by implementing a series of patch antenna arrays. The experiment took five 1 by 4 coaxial-fed patch antenna arrays with elements matched to different levels at different frequencies as source samples. The output model achieves an accuracy of around 84% defined in section III-B, while the regular model reaches only 65%. Also, compared to the regular model only serving for one single target array, the two-order model can cover a series of arbitrary 1 by 4 antenna arrays with similar topology: other coaxial-fed patch antenna arrays at new frequencies, coaxial-fed stacked patch antenna arrays, or coupling-fed patch antenna arrays at arbitrary frequencies. The proposed method can be a competitive alternative tool for designing and analyzing antenna arrays due to its merits of high generalized synthesis capability and low computation cost.

The content is arranged as follows. Section II demonstrates the principle and the workflow of the presented method in detail, followed by instruction and discussion of the implementation on patch antenna arrays in section III. The conclusion is drawn in section IV.

II. TWO-ORDER DL-BASED METHOD

A. Workflow

The workflow of the regular DL-based method and the proposed two-order method are illustrated and compared in Fig. 2. As seen in Fig. 2(a), the conventional DL methods often target one single array and feature at direct rough training with the array excitation conditions and the simulated array radiation of the target sample. Consequently, a demanding simulation workload is obliged to yield the regular models; the standard models are poorly generalized and only applicable to a single target array.

The major improvement of our method is to include several arrays as training samples and propose a two-order training method to arrive at a highly generalized two-order model. Several typical arrays instead of a single target array as training samples ensure a supply of more informative, representative, and diverse array synthesis knowledge. This richer knowledge, of course, upgrades the complexity of learning. For this reason, the two-order learning strategy is proposed as shown in Fig. 2(b).

Inspired and theoretically supported by the conventional EM knowledge, we degrade the complicated learning object to two unmixed tasks: grasping the generic characteristics of radiation synthesis; capturing the detailed radiation variations. The general rules of radiation synthesis hide behind the array factor. Accordingly, to start with, we collect sufficient
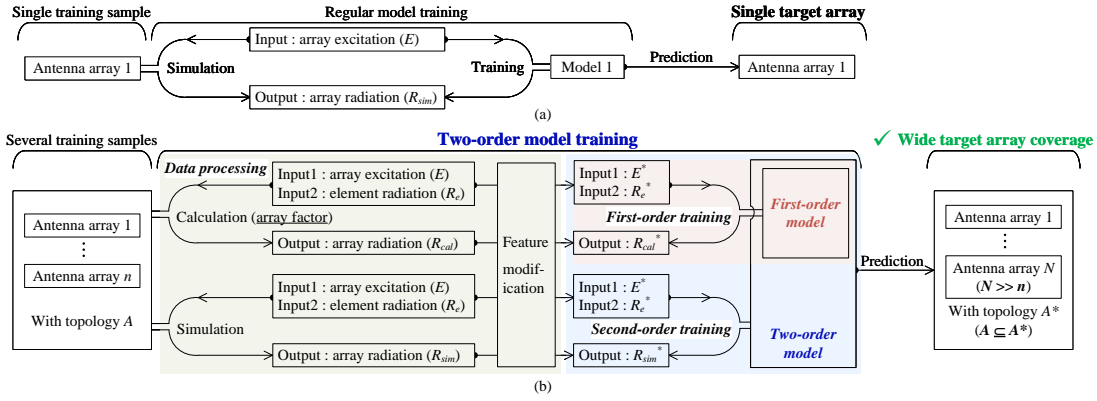
Fig. 2. The principle diagram of (a) regular method and (b) the proposed two-order method.

theoretical data by applying the array factor to train a first-order model. After that, we simulate several customized arrays to gather the complete variated radiation. A two-order model is elevated based on the well-trained first-order model to focus on learning the radiation variances during the second order. Under the first-order model, the two-order model can quickly capture the personalized radiation variations caused by substantial coupling effects in the customized arrays.

Overall, the two-order learning strategy significantly alleviates the burden on simulation and renders the final two-order model with higher generalization ability. As illustrated in Fig. 2(b), its workflow contains three main procedures: data processing, first-order training, and second-order training, which will be demonstrated in detail below.

B. Data Processing

For radiation synthesis of a series of antenna arrays with similar topology, only a limited number of different antenna arrays need to be taken along with their elements as source samples for training. These source samples, utilizing a specific array arrangement, radiation structure, and feeding scheme, work at different frequencies and are matched to different levels to represent most of the target arrays adequately. These source samples then need to go through a calculation based on well-established array factors [30] to collect data for the first-order training and EM simulation for the second-order model.

The data sets for training either model consist of given excitation signals and element radiation patterns as input, and corresponding array radiation patterns as the output label. The only difference is that the calculation carries only the array factor, as seen in Fig. 2(b). The data for training the first-order model contains only generic features related to array factors. In contrast, the data for the second order considers the detailed radiation variations due to concrete coupling effects in the case of a specific array arrangement with different operating frequencies, radiation structures, and feeding schemes. The data from calculation or simulation need to be modified to highlight the features, facilitating the following training. The modification of the excitation signals and radiation patterns differs since they have different physical meanings and data characteristics.

For each set of excitation signals (E), a standard definition is n amplitudes (I) and phases (α):

$$E = [I_1, ..., I_n, \alpha_1, ..., \alpha_n], \qquad (1)$$

where n is the number of ports, I could be any non-negative value, and α may range from $0°$ to $360°$. So, E can have large values and a large positive mean. However, neural networks prefer small values and a zero mean to ensure advanced stability. Thus, E should better be transformed into the complex format by applying Euler's formula, as expressed in:

$$\begin{aligned} E^* &= [Re(Ie^{j\alpha}), Im(Ie^{j\alpha})] \\ &= [[I_1 \cos\alpha_1, I_2 \cos\alpha_2, ..., I_n \cos\alpha_n] \\ &\quad [I_1 \sin\alpha_1, I_2 \sin\alpha_2, ..., I_n \sin\alpha_n]]. \end{aligned} \qquad (2)$$

After transformation, the mean value for excitation (E^*) would be close to zero, and then, after normalization, its magnitude value would be between 0 and 1.

We only take the radiation pattern in one elevation plane where the elements are aligned since it dominates in the linear array. More elevational or azimuthal radiations can be added in case detailed performance matters. The radiation values are usually in decibel format (dB). The decibel format visually shows more precise details within the whole range than the linear format since the proportion of maximum and minimum values is smaller in the decibel format. However, in practice, the values within the main lobe have higher priority than others. Thus, it is better to use linear data to train the model to achieve higher performance within the main lobe. Then, after normalization, the values out of the main lobe would significantly approach zero, and the rest be small positives.

After these modifications, the data sets emphasized their features and are now ready for training. If not explicitly noted, all the following data sets from now on refer to the modified data sets.

C. First-order Training

During training, the first step is using the calculation data to learn the generic features of radiation synthesis. As mentioned above, the data sets for the first-order model are array radiation patterns calculated from the array factor along with given
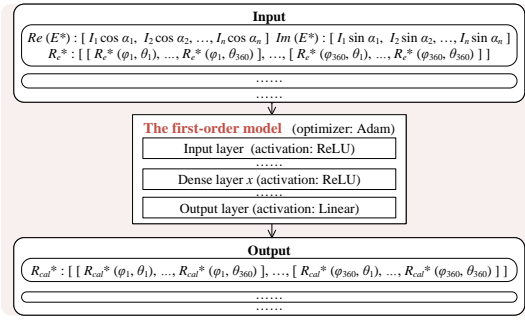
Fig. 3.   The principle diagram of the first-order model.

Fig. 4.   The principle diagram of the final two-order model.

excitation signals and element radiation patterns. Noted that modified array factor or other available formulas can also be applied if adaptive or customized performance is required. For each data set, a set of excitation signals and the element radiation patterns are taken as input; the corresponding calculated array radiation pattern is as output label. Numerically, each input contains two 1 by n (n is the number of elements) vectors for real and imaginary parts of excitation and another vector for element radiation pattern. At the same time, each output is a similar vector for the array radiation patterns. The vector for either element or array radiation pattern can be one-dimensional in the case of the linear array and two-dimensional for the planar array.

With sufficient processed calculation data, a fully-connected DNN, as shown in Fig. 3, is employed to learn the generic features of radiation synthesis. The basic architecture of the first-order model consists of an input layer, an output layer, and several Dense layers as the hidden layers. For optimal performance, possible adjustments include the number of layers, each layer's size and activation function, the optimizer, and other available techniques. Here, the adaptive moment estimate (Adam) is recommended as an optimizer. Adam proposed in [31] combines the advantages of AdaGrad [32] and RMSProp [33] and is well-suited to optimization problems with high-dimensional parameter spaces:

$$Initialize:\quad \beta_1,\ \beta_2,\ \alpha,\ \epsilon,\ g_0,\ G_0,\ G_0^2, \tag{3}$$

$$Gradient:\quad g_i = \nabla Y_i = \nabla F(w_{i-1}^T \cdot X + b_{i-1}), \tag{4}$$

$$1_{st}moment:G_i = [\beta_1 \cdot G_{i-1} + (1-\beta_1) \cdot g_i]/(1-\beta_1^i), \tag{5}$$

$$2_{nd}moment:G_i^2 = [\beta_2 \cdot G_{i-1}^2 + (1-\beta_2) \cdot g_i^2]/(1-\beta_2^i), \tag{6}$$

$$Update:\qquad w_i = w_{i-1} - \alpha \cdot G_i/(\sqrt{G_i^2} + \epsilon). \tag{7}$$

Rectified Linear Unit (ReLU) [34] is taken as activation for each layer, except Linear for the last layer. We choose ReLU because our expected output, the radiation strength, should be positive and continuous float values. At the same time, ReLU is exactly defined as the positive part of its argument:

$$F(X) = Max(0,\ w^T \cdot X + b). \tag{8}$$

Also, ReLU can alleviate vanishing gradient problems. After training using appropriate architecture and techniques, the well-trained first-order model holds the generic radiation synthesis features.
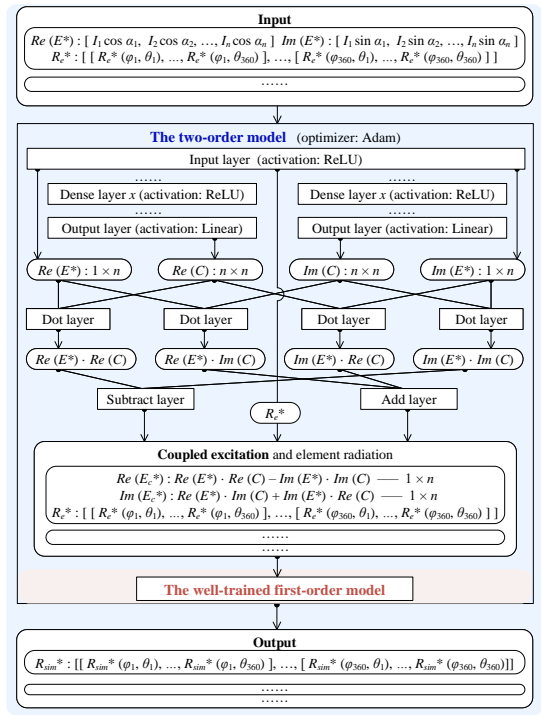
D. Second-order Training

With the well-trained first-order model as a basis, a two-order model is built to further capture the detailed radiation variations due to coupling effects in the case of specific array arrangements with different operating frequencies, radiation structures, and feeding schemes. To summarize, its rough principle is to extract the coupling effects, then compress and integrate them into the original excitation signals, marked as coupled excitation signals, and, at last, feed them along with the element radiation patterns into the well-trained first-order model. Since the well-trained first-order model has already acquired the generic features of radiation synthesis, the final two-order model can better capture the detailed radiation variations due to substantial coupling effects. The absolute architecture of the two-order model is exhibited in Fig. 4, where sharp rectangles represent structures of the model, and rounded ones hold the input, intermediate, or output data.

In practice, as seen in Fig. 4, the extraction and compression of the coupling effects are accomplished by using two separate DNNs with similar architectures: an input layer, an output layer, and several Dense layers as the hidden layers. As for the optimizer and activation function, the consideration is the same as what we discussed for the first-order model since these two-order models share the same final goal: Adam is again utilized as the optimizer; ReLU is taken as the activation function.

These two DNNs manage to reveal and compress the coupling information behind the input−−the excitation signals (E^*) and the element radiation patterns (R_e^*)−−into two n by n vectors, standing for the real ($Re(C)$) and imaginary ($Im(C)$) parts of an assumed complex coupling factor (C), respectively. The size of the coupling factor being confined as n by n is supported by a reasonable assumption that, given any certain

This article has been accepted for publication in IEEE Transactions on Artificial Intelligence. This is the author's version which has not been fully edited and content may change prior to final publication. Citation information: DOI 10.1109/TAI.2022.3192505

ZHAO ZHOU *et al.*: TWO-ORDER DEEP LEARNING FOR GENERALIZED SYNTHESIS OF RADIATION PATTERNS FOR ANTENNA ARRAYS   5

excitation condition, the coupling effect between every two elements can be approximately transferred and generalized into a complex port-to-port coefficient. For example, the two values at row i and column j of $Re(C)$ and $Im(C)$ together evaluate the coupling influence of element i on element j and vice versa.

The two DNNs are then followed with Dot layer, Add layer, and Subtract layer as shown in Fig. 4. These operation layers are employed to execute the complex multiplication of E^* and C. This step is to integrate the extracted coupling factor into the original excitation signals, forming so-called coupled excitation signals. The actual multiplication here is divided into several separate operations on their real and imaginary vectors ($Re(E^*)$, $Im(E^*)$, $Re(C)$, $Im(C)$).

Finally, the well-trained first-order model is attached to the posterior end of the whole architecture. The coupled excitation signals yielded from the afore-mentioned operation layers, along with the element radiation patterns, are fed into the well-trained first-order model for the second-order training. The actual radiation patterns from simulation or measurement results are used as label data. For simulation, we set up the array in the virtual EM environment supported by Computer Simulation Technology (CST) Studio Suite® and then proceed with its frequency domain solver to yield the data. Since the well-trained first-order model has mastered the generic features of radiation synthesis in advance, it is easier for the second-order training to capture the detailed radiation variations, probably leading to high generalization ability, performance, and robustness.

III. IMPLEMENTATION ON PATCH ANTENNA ARRAYS

We validated the proposed two-order method's feasibility, high generalization ability, and performance on a series of patch antenna arrays. Expressly, five 1 by 4 coaxial-fed patch antenna arrays at different frequencies, along with their elements, are set as training samples. (We use a 1 by 4 patch antenna array as the test vehicle for no particular reason, consider it an example to testify our method.) The final two-order model was proven superior to the regular deep learning model and capable of generalized synthesis of radiation patterns of a series of 1 by 4 arrays, including coaxial-fed patch antennas at other different frequencies and stacked patch antennas and coupling-fed patch antennas at arbitrary frequencies.

Next, we will demonstrate the training process, including data processing, the first and second-order training, a comparison with the regular deep learning model, and the verification of three cases.

A. Data Processing

We simulated five coaxial-fed patch antennas well-matched at different frequencies via CST to collect their element radiation patterns. And they made up five 1 by 4 arrays at around half-wavelength distance. Fig. 5 shows the structure of the element and array. The parameters and characteristics in all five cases are listed in Table I. Then, each array went through pattern multiplication based on the array factors to generate 10000 sets of array radiation patterns for the first-order model,
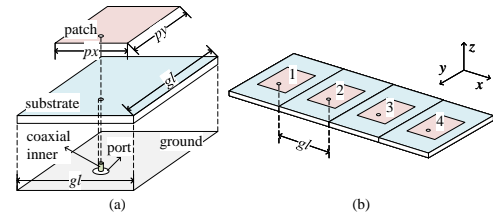

Fig. 5.   The structures of the source samples. (a) Element. (b) Array. (*Note: The substrate used FR-4 with an ϵ_r of 4.4 and a thickness of 1 mm.)

TABLE I
THE PARAMETERS AND CHARACTERISTICS OF SOURCE SAMPLE ELEMENTS

Sample No.	Freq. (GHz)	Parameters (mm)				S_{11} (dB)	Gain (dBi)	HPBW (deg)
		gl	px	py	df			
1	0.95	150	83.9	75.2	12	−14.8	6.75	94.3
2	1.94	75	40.8	36.5	7.5	−22.6	6.68	95.3
3	2.96	50	24.1	24	4	−15.9	6.6	96.3
4	4	37.5	17.8	17.7	2.7	−14.2	6.53	97.1
5	4.94	30	17.5	14.1	1.9	−34.9	6.62	93.8

(*Note: Freq. means the operating frequency;
HPBW means half-power beamwidth;
S_{11}s, Gains, and HPBWs are at the operating frequency.)

with various excitation conditions――the amplitudes varied from 0 to 1.5 at a step of 0.5 and the phases from $0°$ to $180°$ at a step of $20°$ given. Likewise, it underwent simulation via CST to collect 5000 sets for training the second model. There were 50000 sets for the first order and 25000 sets for the second order. It is worth mentioning that the calculation data outnumbers the simulation data because the calculation takes much less time. It took just 1 minute to collect the 50000 sets of calculation data and roughly 108 hours and 20 minutes to collect 25000 sets of simulation data for the second-order model. The amounts of data sets for the first and second orders are negotiable. In general, more data sets probably lead to higher accuracy. Thus, the portions here mainly depend on the tolerance range of accuracy. Then, as demonstrated in section II-B, we modified the collected raw data sets to highlight the features before training. The data set for each excitation condition was two 1 by 4 vectors, and each radiation pattern of either the element or array was 1 by 360. Thus, each input was two 1 by 4 vectors along with one 1 by 360 vector, and the output was one 1 by 360 vector for either the first or the second-order model training.

B. First-order Training

Within the 50000 sets of calculated array radiation patterns, we took 70%, 35000 sets as output labels, their corresponding excitation conditions and element radiation patterns as input for the first-order training, and the rest 30% data for testing. After careful adjustment, the first-order model was fixed, as illustrated in Fig. 6. In practice, this model had four hidden layers, holding 750, 550, 1550, and 1350 neurons, respectively. Fig. 8(a) shows the accuracy during training and testing. The accuracy reached 90.20% during training and 89.61% for testing.

Note that the accuracy mentioned in this article is the proportion of the radiation pattern values where the difference between prediction and simulation meets the predefined criteria, no more than $0.5\,\mathrm{dB}$ for positive values and $1\,\mathrm{dB}$ negative
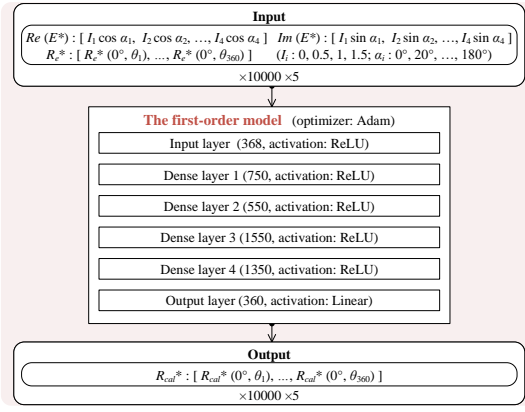
Fig. 6.   The instance structure of the first-order model in this case.

ones. Thus, although the accuracy may not seem that high, a good agreement has been achieved, verified, and observed in the following comparison between simulation and prediction results.

C. Second-order Training

Similarly, we took 70 %, 17500 sets of the simulated array radiation patterns as output labels, along with their related excitation conditions and element radiation patterns as input for the second-order training and the rest for testing. With the well-trained first-order model from section III-B as a basis, the final two-order model was built and shown in Fig. 7. In the final model, the sub-models to predict the real and imaginary parts of the assumed coupling factor share the same architecture, also four hidden layers with 750, 700, 1150, and 1600 neurons.

The accuracy of the final two-order model is shown in Fig. 8(b), which shares the exact definition from section III-B. The final model showed its optimal performance with an accuracy of 84.57% during training and 83.52% for testing. One might notice that the accuracy of the final model is lower than that of the first-order model by around 12%, which is reasonable as the second-order training use much fewer data sets than the first order. But again, the achieved accuracy is considered high according to its definition.

D. Verification

The two-order model for radiation synthesis of a series of 1 by 4 patch antenna arrays has been obtained. It was then applied to other 1 by 4 patch antenna arrays than the source samples to verify its performance and robustness. The cases for verification take into account the most typical variations in array designs, like operating frequency, radiator structure, and feeding scheme. In practice, we arbitrarily chose a 1 by 4 coaxial-fed patch antenna array at $3.48\,\mathrm{GHz}$, a 1 by 4 stacked patch antenna array at around $1.5\,\mathrm{GHz}$, and a 1 by 4 coupling-fed patch antenna array at $2.41\,\mathrm{GHz}$ for the validation. Also, we validated our model with a published microstrip antenna from [35]; for experimental validation, the proposed method was testified on an antenna array prototype from our published work in [36].
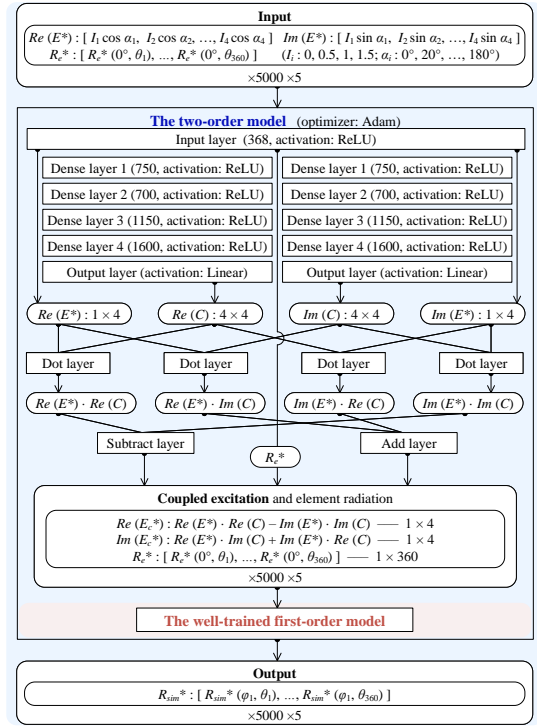

Fig. 7.   The instance structure of the second-order model in this case.
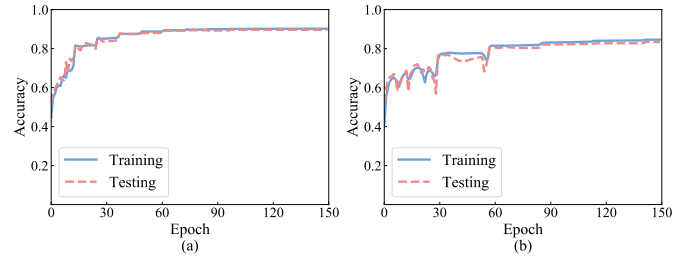

Fig. 8.   The accuracy of (a) the first-order and (b) the second-order model.

TABLE II
THE PARAMETERS AND CHARACTERISTICS OF ELEMENT IN CASE I

Freq.	Parameters (mm)				S_{11}	Gain	HPBW
(GHz)	gl	px	py	df	(dB)	(dBi)	(deg)
3.48	42.8	20.5	20.4	3.2	-14.4	6.56	96.3

1) Case I: The first case is a 1 by 4 coaxial-fed patch antenna array working at $3.48\,\mathrm{GHz}$. It has the same structure as the source samples shown in Fig. 5. The fixed parameters and basic characteristics of its elements are listed in Table II. With its element radiation pattern and an arbitrary excitation condition fed into the model, the model was proven to give the predicted array radiation pattern that matches perfectly with the simulation result. Fig. 9 shows the calculated, simulated, and predicted array radiation patterns given one certain random excitation condition listed beside.

Note that the predicted radiation pattern output from the two-order model is initially in the linear format as we used linear data for training. The prediction is transformed into decibel format to compare with simulation and calculation. A noticeable difference between the simulation and calculation can be observed. The prediction result can ideally correct this difference and agree with the simulation.
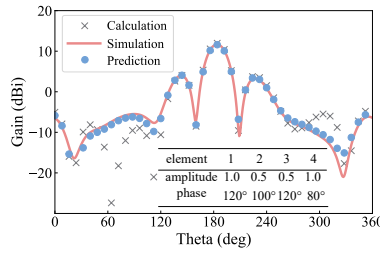
Fig. 9. A comparison between the calculated, simulated, and predicted array radiation patterns given a certain excitation condition in case I.
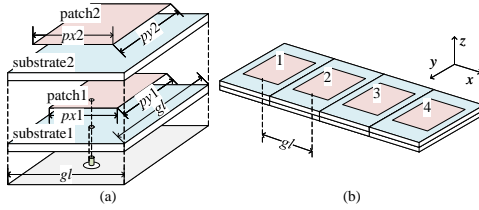

Fig. 10. The structure of the stacked patch antenna for verification in case II. (a) Radiation element. (b) 1 by 4 array.
(*Note: The substrate1&2 used FR-4 with an ϵ_r of 4.4 and a thickness of 1 mm.)

TABLE III
THE PARAMETERS AND CHARACTERISTICS OF ELEMENT IN CASE II

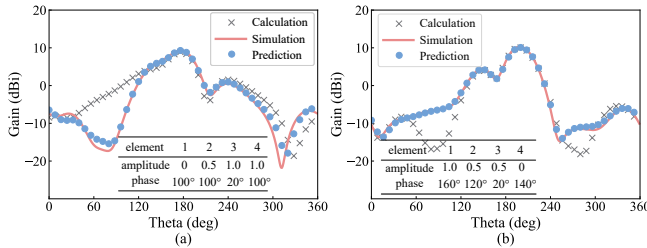| Freq.	Parameters (mm)						S$_{11}$	Gain	HPBW
(GHz)	gl	px1	py1	px2	py2	df	(dB)	(dBi)	(deg)
1.47	100	49	46	50	48	1.6	−11.3	6.56	95.3
1.54	100	49	46	50	48	1.6	−22.4	6.68	92.8

Fig. 11. A comparison between the calculated, simulated, and predicted stacked patch array radiation patterns given a certain excitation conditions in case II at (a) 1.47 GHz and (b) 1.54 GHz.

2) Case II: The second case is a 1 by 4 stacked patch antenna array working around 1.5 GHz to test its robustness in terms of radiator structure. It uses a two-layer patch as its radiator, which is widely applied in patch antenna designs to expand its bandwidth, and it is exhibited in Fig. 10. Since the two-layer patch antenna can resonate at two frequencies, Table III shows the element's parameters and characteristics at their two operating frequencies, 1.47 GHz and 1.53 GHz. And the results for radiation synthesis at both frequencies are presented in Fig. 11. At both frequencies, the predictions match pretty well with the simulations when excited by the random excitation signals and outperform the calculations.

3) Case III: In this case, we took a 1 by 4 coupling-fed patch antenna array working at 2.41 GHz to prove its compatibility with feeding techniques. Here, the patch is coupling-fed by an L-shaped strip instead of directly fed by a coaxial cable. This coupling-fed approach is a common alternative feeding way for bandwidth enhancement. Its structure,
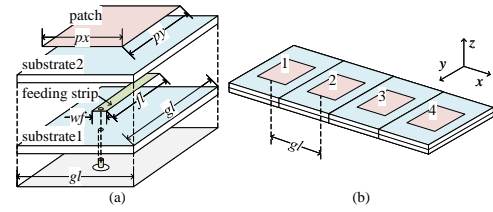

Fig. 12. The structure of the coupling-fed patch antenna in case III. (a) Element. (b) Array.
(*Note: The substrate1&2 used FR-4 with an ϵ_r of 4.4 and a thickness of 1 mm.)

TABLE IV
THE PARAMETERS AND CHARACTERISTICS OF ELEMENT IN CASE III

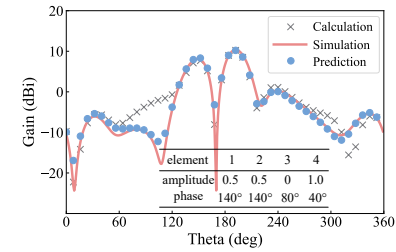| Freq.	Parameters (mm)					S$_{11}$	Gain	HPBW
(GHz)	gl	px	py	wf	lf	df	(dB)	(dBi)	(deg)
2.41	60	28.8	28.8	1.5	14	1	−18.3	6.43	98.4

Fig. 13. A comparison between the calculated, simulated, and predicted coupling-fed array radiation patterns given certain excitation conditions in case III.
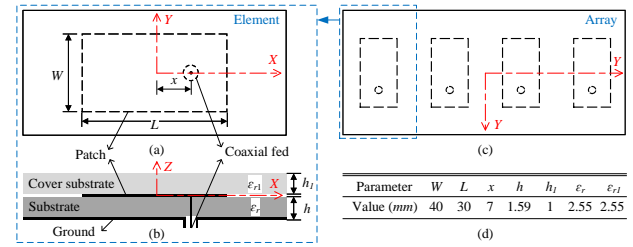

Fig. 14. The structure of the dielectric-covered patch antenna in case IV: (a)top view and (b) side view of the Element; (c) top view of the array; (d) coefficients table.

parameters, and characteristics can be found in Fig. 12 and Table IV, respectively. And also, Fig. 13 shows one of the verification results. Generally, a high matching level between the prediction and simulation can be observed, proving that the model works well even with modified feeding techniques.

4) Case IV: We validated our two-order model on a published microstrip antenna from [35]. It is a classical coaxial-fed microstrip antenna covered with an extra dielectric layer to prevent environmental influences, as seen in Fig. 14. The dielectric layer can also affect the antenna's EM performance by lowering the resonate frequency. According to the coefficients provided in [35], we set up the antenna element and the corresponding array in CST to collect the required simulation data. Then we utilized our model to predict its array radiation. The comparison result is exhibited in Fig. 15. We can observe that the predicted radiation agrees well with the simulation radiation.

5) Experimental validation: For experimental validation, we proceeded with the proposed method on an antenna array
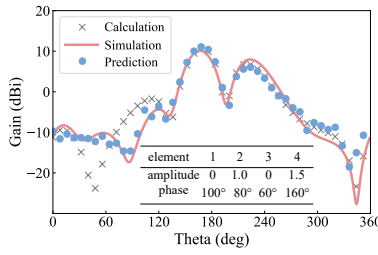
Fig. 15. A comparison between the calculated, simulated, and predicted coupling-fed array radiation patterns given certain excitation conditions in case IV.
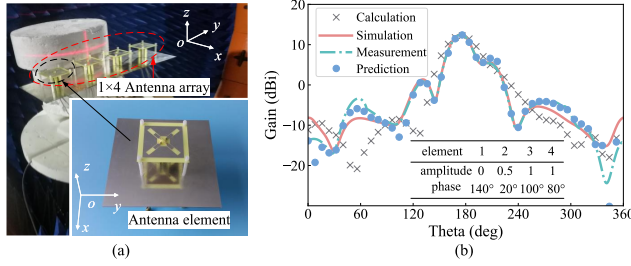

Fig. 16. (a) Experimental setup. (b) A comparison between the calculated, simulated, measured, and predicted coupling-fed array radiation patterns given certain excitation conditions in experimental validation.

TABLE V
THE COMPARISON OF TIME CONSUMPTION OF REGULAR METHOD AND THE PROPOSED TWO-ORDER METHOD

	Target arrays	Training samples	Time			
			Cal. data	Sim. data	Training	In total
Pro.	N	n (= 5)	1m×5	21h40m×5	(18m+16m)×5	21h31m×5
Reg.	N	N	——	43h20m×N	7m×N	43h27m×N

(*Note: Usually $N \gg n$;
       Pro. represents the proposed two-order method;
       Reg. represents the regular method.)

prototype from our previous work [36]. We have the array prototype measured using a SATIMO multi/probe spherical near-field system. The antenna prototype was initially designed as a slant dual-polarization corresponding to two ports. During the experiment, we fed identical signals to each pair of ports to make it operate in the patch mode. Fig. 16 compares its calculation, simulation, measurement, and prediction array radiation on an arbitrary excitation state. The prediction here is based on measured element radiation. It is safe to say that the prediction radiation approximately equals the experimental result despite a bit of variance of less than 3 dB outside the main lobe.

We have far tested the well-trained two-order model in five cases and verified its high generalization ability, performance, and robustness.

E. Comparison and discussion

To quantify our improvement over the existing regular deep learning synthesis methods [26–28], we compare the proposed model to the typical model, as shown in Fig. 17, regarding the accuracy and the total time consumption. Fig. 18 exhibits their accuracy when being trained with one array sample; Table V lists the detailed time consumption over their training process. Our quantitative advantages can be summed up in
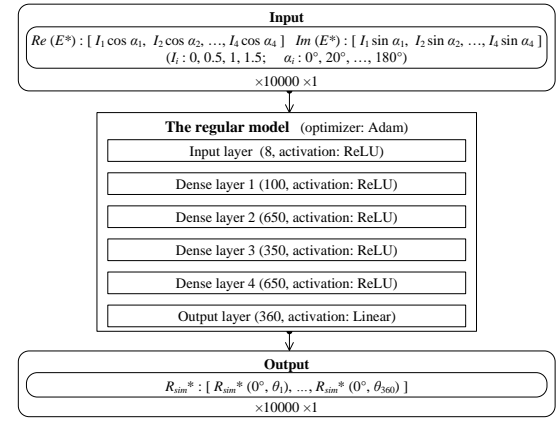

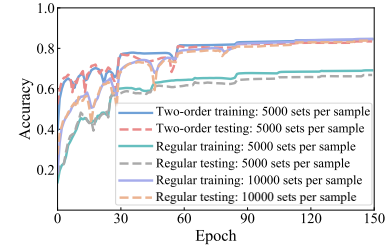Fig. 17. The architecture of regular model.

Fig. 18. The accuracy of regular model and the proposed two-order model.

three aspects. For one thing, we cut down nearly half of the simulation needed to tackle each training sample. It turns out that, with 5000 sets of simulation data per sample, the traditional method can only reach an accuracy up to 65 %. In contrast, the proposed two-order method realizes about 84 %. The standard method requires double the amount (10000 sets) of simulation to achieve the same level of accuracy (around 83 %). Therefore, our method saves nearly half of simulation time for each training sample, which means a lot since the simulation occupies over 99 % of time for the regular model. For the second point, we significantly reduce the number of training samples needed for covering the exact scaled N target arrays, thereby freeing a huge amount (Nn) of simulation workload. The last merit is that after a once two-order training process, the two-order model of high generalization ability can solve N target arrays' synthesis problem once and for all. In contrast, the traditional methods have to repetitively produce N models for different target arrays. Here, N depends on the training samples' informativeness, representativeness, and diversity. N can hardly be quantified because the generalized two-order model covers a continuous target array space rather than one single target array like the traditional methods do. Thus, the proposed two-order approach takes much less time to provide a more generalized synthesis solution than the existing regular methods.

This framework can also be expected to outperform traditional methods in the case of the planar array. The main difference is that the planar array must consider radiations over at least two elevation planes instead of one for the linear array. Therefore, we must adopt an advanced feature extraction scheme to compress the complex data. Accordingly, the size of data and the number of hidden layers and neurons should

increase.

IV. CONCLUSION

This letter proposed a two-order deep learning method to generalize radiation synthesis of a series of antenna arrays with similar topology. This method uses the well-established array factor to learn the generic features of radiation synthesis using the first order. Then the second order focuses on further capturing the detailed radiation variations caused by concrete coupling effects in the case of a specific array arrangement with different operating frequencies, radiation structures, and feeding schemes. Compared with most published deep learning methods, this method has higher generalization ability, performance, and robustness, which has been testified with an implementation on a series of patch antenna arrays. The two-order model can synthesize a series of 1 by 4 patch antenna arrays with different operating frequencies, radiation structures, and feeding schemes at an accuracy of around 84%. In beyond-5G/6G scenarios where multiple antenna arrays co-exist in each single base station, we can utilize the proposed model to conveniently monitor all the arrays' radiation patterns.

REFERENCES

[1] Y. Jin, J. Zhang, S. Jin, and B. Ai, "Channel estimation for cell-free mmwave massive mimo through deep learning," *IEEE Transactions on Vehicular Technology*, vol. 68, no. 10, pp. 10 325–10 329, 2019.
[2] A. S. Alwakeel and A. H. Mehana, "Data-aided channel estimation for multiple-antenna users in massive mimo systems," *IEEE Transactions on Vehicular Technology*, vol. 68, no. 11, pp. 10 752–10 760, 2019.
[3] Y. Liao, Y. Hua, and Y. Cai, "Deep learning based channel estimation algorithm for fast time-varying mimo-ofdm systems," *IEEE Communications Letters*, vol. 24, no. 3, pp. 572–576, 2019.
[4] C. Lu, W. Xu, S. Jin, and K. Wang, "Bit-level optimized neural network for multi-antenna channel quantization," *IEEE Wireless Communications Letters*, vol. 9, no. 1, pp. 87–90, 2019.
[5] X. Wei, C. Hu, and L. Dai, "Deep learning for beamspace channel estimation in millimeter-wave massive mimo systems," *IEEE Transactions on Communications*, 2020.
[6] E. Balevi, A. Doshi, and J. G. Andrews, "Massive mimo channel estimation with an untrained deep neural network," *IEEE Transactions on Wireless Communications*, vol. 19, no. 3, pp. 2079–2090, 2020.
[7] Y. Zhang, Y. Mu, Y. Liu, T. Zhang, and Y. Qian, "Deep learning-based beamspace channel estimation in mmwave massive mimo systems," *IEEE Wireless Communications Letters*, vol. 9, no. 12, pp. 2212–2215, 2020.
[8] Y. Sui, Y. He, T. Cheng, Y. Huang, and S. Ning, "Broad echo state network for channel prediction in mimo-ofdm systems," *IEEE Transactions on Vehicular Technology*, vol. 69, no. 11, pp. 13 383–13 399, 2020.
[9] M. E. Morocho-Cayamcela, M. Maier, and W. Lim, "Breaking wireless propagation environmental uncertainty with deep learning," *IEEE Transactions on Wireless Communications*, vol. 19, no. 8, pp. 5075–5087, 2020.
[10] W. Ma, C. Qi, Z. Zhang, and J. Cheng, "Sparse channel estimation and hybrid precoding using deep learning for millimeter wave massive mimo," *IEEE Transactions on Communications*, vol. 68, no. 5, pp. 2838–2849, 2020.
[11] Z.-M. Liu, C. Zhang, and S. Y. Philip, "Direction-of-arrival estimation based on deep neural networks with robustness to array imperfections," *IEEE Transactions on Antennas and Propagation*, vol. 66, no. 12, pp. 7315–7327, 2018.
[12] H. Huang, J. Yang, H. Huang, Y. Song, and G. Gui, "Deep learning for super-resolution channel estimation and doa estimation based massive mimo system," *IEEE Transactions on Vehicular Technology*, vol. 67, no. 9, pp. 8549–8560, 2018.
[13] Y. Cao, T. Lv, Z. Lin, P. Huang, and F. Lin, "Complex resnet aided doa estimation for near-field mimo systems," *IEEE Transactions on Vehicular Technology*, vol. 69, no. 10, pp. 11 139–11 151, 2020.

[14] L. Li, L. G. Wang, F. L. Teixeira, C. Liu, A. Nehorai, and T. J. Cui, "Deepnis: Deep neural network for nonlinear electromagnetic inverse scattering," *IEEE Transactions on Antennas and Propagation*, vol. 67, no. 3, pp. 1819–1825, 2018.
[15] H. M. Yao, E. Wei, and L. Jiang, "Two-step enhanced deep learning approach for electromagnetic inverse scattering problems," *IEEE Antennas and Wireless Propagation Letters*, vol. 18, no. 11, pp. 2254–2258, 2019.
[16] Y. Zhou, Y. Zhong, Z. Wei, T. Yin, and X. Chen, "An improved deep learning scheme for solving 2d and 3d inverse scattering problems," *IEEE Transactions on Antennas and Propagation*, 2020.
[17] H. Zhou, T. Ouyang, Y. Li, J. Liu, and Q. Liu, "Linear-model-inspired neural network for electromagnetic inverse scattering," *IEEE Antennas and Wireless Propagation Letters*, vol. 19, no. 9, pp. 1536–1540, 2020.
[18] K. Xu, L. Wu, X. Ye, and X. Chen, "Deep learning-based inversion methods for solving inverse scattering problems with phaseless data," *IEEE Transactions on Antennas and Propagation*, vol. 68, no. 11, pp. 7457–7470, 2020.
[19] Z. Ma, K. Xu, R. Song, C.-F. Wang, and X. Chen, "Learning-based fast electromagnetic scattering solver through generative adversarial network," *IEEE Transactions on Antennas and Propagation*, 2020.
[20] Z. Wei and X. Chen, "Uncertainty quantification in inverse scattering problems with bayesian convolutional neural networks," *IEEE Transactions on Antennas and Propagation*, 2020.
[21] L.-Y. Xiao, W. Shao, X. Ding, Q. H. Liu, and W. T. Joines, "Multigrade artificial neural network for the design of finite periodic arrays," *IEEE Transactions on Antennas and Propagation*, vol. 67, no. 5, pp. 3109–3116, 2019.
[22] J. Jiang and J. A. Fan, "Simulator-based training of generative neural networks for the inverse design of metasurfaces," *Nanophotonics*, vol. 9, no. 5, pp. 1059–1069, 2020.
[23] P. Naseri and S. V. Hum, "A generative machine learning-based approach for inverse design of multilayer metasurfaces," *arXiv preprint arXiv:2008.02074*, 2020.
[24] S. Mishra, R. N. Yadav, and R. P. Singh, "Directivity estimations for short dipole antenna arrays using radial basis function neural networks," *IEEE Antennas and Wireless Propagation Letters*, vol. 14, pp. 1219–1222, 2015.
[25] L. Yuan, X.-S. Yang, C. Wang, and B.-Z. Wang, "Multibranch artificial neural network modeling for inverse estimation of antenna array directivity," *IEEE Transactions on Antennas and Propagation*, vol. 68, no. 6, pp. 4417–4427, 2020.
[26] R. G. Ayestaran and F. Las-Heras, "Obstacle modeling in array synthesis using neural networks," *IEEE Transactions on Antennas and Propagation*, vol. 54, no. 8, pp. 2420–2424, 2006.
[27] R. G. Ayestaran, F. Las-Heras, and L. F. Herrán, "Neural modeling of mutual coupling for antenna array synthesis," *IEEE Transactions on Antennas and Propagation*, vol. 55, no. 3, pp. 832–840, 2007.
[28] J. H. Kim and S. W. Choi, "A deep learning-based approach for radiation pattern synthesis of an array antenna," *IEEE Access*, vol. 8, pp. 226 059–226 063, 2020.
[29] A. Jagannath, J. Jagannath, and T. Melodia, "Redefining wireless communication for 6g: Signal processing meets deep learning with deep unfolding," *IEEE Transactions on Artificial Intelligence*, vol. 2, no. 6, pp. 528–536, 2021.
[30] C. A. Balanis, *Antenna theory: analysis and design*. John wiley & sons, 2015.
[31] D. P. Kingma and J. Ba, "Adam: A method for stochastic optimization," *arXiv preprint arXiv:1412.6980*, 2014.
[32] J. Duchi, E. Hazan, and Y. Singer, "Adaptive subgradient methods for online learning and stochastic optimization." *Journal of machine learning research*, vol. 12, no. 7, 2011.
[33] T. Tieleman, G. Hinton *et al.*, "Lecture 6.5-rmsprop: Divide the gradient by a running average of its recent magnitude," *COURSERA: Neural networks for machine learning*, vol. 4, no. 2, pp. 26–31, 2012.
[34] V. Nair and G. E. Hinton, "Rectified linear units improve restricted boltzmann machines," in *Icml*, 2010.
[35] G. Kumar and K. P. Ray, *Broadband microstrip antennas*. Artech house, 2003.
[36] Z. Zhou, Z. Wei, Z. Tang, Y. Yin, and J. Ren, "Compact and wideband differentially fed dual-polarized antenna with high common-mode suppression," *IEEE Access*, vol. 7, pp. 108 818–108 826, 2019.